INVESTIGATION OF TIME-OF-FLIGHT (TOF) IMAGING SYSTEM DURING DEEP INSPIRATION BREATH-HOLD RADIOTHERAPY (DIBH-RT) FOR LEFT BREAST CANCER PATIENTS

ABUBAKAR AUWAL

UNIVERSITI SAINS MALAYSIA

2022

INVESTIGATION OF TIME-OF-FLIGHT (TOF) IMAGING SYSTEM DURING DEEP INSPIRATION BREATH-HOLD RADIOTHERAPY (DIBH-RT) FOR LEFT BREAST CANCER PATIENTS

by

ABUBAKAR AUWAL

Thesis submitted in fulfilment of the requirements
for the degree of
Doctor of Philosophy

April 2022

ACKNOWLEDGEMENT

I would like to express my gratitude to the Almighty Allah for His guidance and support throughout my Ph.D. journey. I am grateful to my main supervisor, Dr. Mohd Hafiz Mohd Zin for his unwavering support and contribution. This thesis would not have been successful without his critical feedback, support, and constant encouragement. My heartfelt appreciation to my co-supervisors; Dr. Shazril Imran Ibn Shaukat and Dr. Noor Khairiah Binti A. Karim for their immense contributions. My deepest gratitude also goes to the entire Radiotherapy staff at Advanced Medical and Dental Institute for their kindness and assistance during my stay in the department. My senior colleague Lim, I appreciate your help.

I am indebted to my institutions the University of Maiduguri and the University of Maiduguri Teaching Hospital as well as the Nigerian government for financing this study through TETFUND. Special thanks to both current and recent past Chief Medical Directors of the University of Maiduguri Teaching Hospital, Professor Ahmad Ahidjo and Professor Abdurrahman Tahir for the advice, guidance, and unconditional support throughout my career. A big thanks to Dr. Nwobi for the teachings and mentorship since my undergraduate days till date.

I lack words to appreciate my late granny, Mamma Idi for the unconditional love and support rendered to me when they were most needed. To my parents Hajiya Fatimah Yusuf and Alhaji Abubakar Suleiman as well as my Uncle Alhaji Usman Yusuf, I thank you for your prayers and for being a source of support and encouragement. My wife Aishatu Usman Yusuf and the kids, I appreciate your support and sacrifice. To my academic and clinical colleagues back home, I thank you for your patience and understanding.

TABLE OF CONTENTS

LIST OF TABLES

LIST OF FIGURES

Page

LIST OF SYMBOLS

$\bar{x}i$	Individual systematic error
$\sum$	Mean Setup error
$\mu\beta_{EPID}$	Mean breath-hold depth measurements on the sequence of EPID images
$\mu\beta_{TOF}$	Mean breath-hold depth measurements on the sequence of ToF images
A	Amplitude
B	Offset
c	Speed of light
¢	Correction factor
$¢\acute{M}_{BG}$	Correction factor for medial field using background correction method
$¢\acute{M}_{FB}$	Correction factor for medial field using FB correction method
$¢\acute{S}_{BG}$	Correction factor for SCF field using background correction method
$¢\acute{S}_{FB}$	Correction factor for SCF field using FB correction method
d	Depth measurement
$D_{DIBH-MC}$	Breath-hold mark to couch distance
d_s	Measured depth shift
f	Frequency
Hor-$D_{FB-DIBH}$	Free-breathing to breath-hold mark distance along the horizontal axis
i	isocentre
$\tilde{I}_x$	2D Mean image
$\underset{\smile}{I}_{x.}$	2D SD image
$\acute{L}_{BG}$	Average of lateral field ToF image after background segmentation
$\acute{L}_{FB}$	Free-breathing baseline for lateral field
$\acute{M}_{BG}$	Average of medial field ToF image after background segmentation
M_{DIBH}	Deep inspiration breath-hold mark

M_{FB}	Free-breathing mark
$\acute{M}_{FB}$	Small baseline for medial field
M_{pop}	Population mean
Q	Charge
$\acute{S}_{BG}$	Average of SCF field ToF image after background segmentation
$\acute{S}_{FB}$	Small baseline for SCF field
t	Time
Vert-$D_{FB\text{-}DIBH}$	Free-breathing to breath-hold distance mark along vertical axis
x0	Depth at isocentre
xg	Ground truth depth
xs	Depth at shift position
β_{EPID}	Breath-hold depth measurement on single EPID image
β_{TOF}	Breath-hold depth measurement on single ToF image
π	pi
σ_i	Individual random error
φ	Phase shift

LIST OF ABBREVIATIONS

2D	Two-dimensional
3D-CRT	Three-dimensional conformal radiotherapy
ABC	Active breathing coordinator
ADC	Analogue-to-digital converter
AMCW-ToF	Amplitude modulated continuous wave ToF
AP	Anterior-posterior
BB	Ball bearing
BCS	Breast conserving surgery
BH	Breath-hold
BMI	Body mass index
BSA	Body surface area
CBCT	Cone-beam computed tomography
CCD	Cardiac contact distance
CCD	Charge-coupled devices
CCTV	Closed-circuit television
CMOS	Complementary Metal Oxide Semiconductor
CSD	Chest surface displacement
CT	Computed tomography
DIBH-RT	Deep inspiration breath-hold radiotherapy
DIBH	Deep inspiration breath-hold
DRR	Digitally reconstructed radiograph
eNAL	Extended no action level
EPID	Electronic portal imaging device
FB	Free-breathing

FOV	Field-of-view
fps	Frame per second
HF-FE	Heart position to field edge
HNC	Head and neck cancer
IGRT	Image-guided radiotherapy
IMRT	Intensity Modulated Radiotherapy
IR	Infrared
kV	kiloVoltage
laser	light amplification by the stimulated emission of radiation
LED	Light-emitting diode
mA	milli ampere
mAs	milli ampere second
MHD	Maximum heart distance
MHz	Mega Hertz
MLC	Multi-leaf collimator
ms	milli second
MV	MegaVoltage
NAL	No action level
NIR	Near-infrared light
PBI	Partial breast irradiation
PB-ToF	Pulse-based ToF
PSD	Patient surface depth
PTV	Planning target volume PTV
QA	Quality assurance
ROI	Region of interest
RPM	Real-time position management

RTOG	Radiation Therapy Oncology Group
SAD	Source-to-axis distance
SCF	supraclavicular fossa
SD	Standard deviation
SGRT	Surface guided radiotherapy
SI	Superior-inferior
SIS	Surface imaging system
TPS	Treatment planning system
VMAT	Volumetric Modulated Arc Therapy
XVI	X-ray Volumetric Imaging

LIST OF APPENDICES

PENYIASATAN SISTEM PENGIMEJAN MASA-TERBANG (TOF) SEMASA RADIOTERAPI PENARIKAN TAHAN-NAFAS DALAM (DIBH-RT) UNTUK PESAKIT KANSER PAYUDARA KIRI

ABSTRAK

Radioterapi Penarikan Tahan-Nafas Dalam (DIBH-RT) memerlukan pesakit menarik dan menahan nafas dalam semasa rawatan. Proses ini menolak jantung daripada medan rawatan dan mengurangkan dos jantung sebanyak lebih 50%. Walau bagaimanapun, kebolehulangan dan kestabilan penahanan nafas semasa DIBH-RT boleh menjejaskan kejayaan rawatan. Tujuan kajian ini adalah untuk mengkaji aplikasi sistem pengimejan masa terbang (ToF) untuk memantau penahanan nafas semasa DIBH-RT. Argos P330 3D ToF Camera (Bluetechnix Austria) dicirikan dengan pengimejan fantom ISOCube untuk menilai kestabilan pengukuran ToF bersama dengan CBCT. Selepas itu, pengimejan ToF dilakukan serentak dengan CBCT untuk 13 pesakit DIBH-RT bagi pengesahan kedudukan pesakit. Sesaran permukaan dada dianggarkan daripada setiap modaliti dan dibandingkan untuk mengesahkan ukuran daripada ToF. Pengimejan ToF juga dilakukan serentak dengan pengimejan cine EPID untuk pengesahan kestabilan dan kebolehulangan tahan nafas semasa rawatan. Data dianalisis menggunakan MATLAB (MathWorks, Natick, MA) dan ujian statistik telah dilakukan untuk penilaian ketepatan ToF. Kestabilan pengukuran intra-pesakit bagi sistem ToF berjulat dari 0.05 hingga 0.31 mm manakala bagi inter-pesakit berjulat antara 0.68 hingga 0.74 mm apabila diukur dengan fantom. Perbezaan purata mutlak antara ToF dan CBCT ialah 0.28 ± 0.90 mm, dan korelasi 0.96 dengan had persetujuan (LOA) sebanyak -1.49, 2.04 mm menggunakan fantom. Keputusan yang diperoleh daripada pesakit ialah 2.88 ± 5.89 mm, 0.92, dan -7.36, 1.60 mm. Purata korelasi yang diperolehi antara ToF dan EPID ialah -0.84. Purata kebolehulangan dalam medan adalah 2.7 mm, 1.37 mm, dan 1.17 mm untuk medan sisi, medial dan SCF, masing-masing. Purata kebolehulangan dan kestabilan dalam pecahan adalah 3.74 mm, dan 0.8 mm, masing-masing menunjukkan kebolehulangan yang baik. Sistem pengimejan ToF menunjukkan ketepatan yang baik untuk memantau penahanan nafas semasa DIBH-RT dengan perbezaan purata sebanyak 2.88±5.89 mm berbanding CBCT. Oleh itu, ToF boleh digunakan dengan selamat semasa pengesahan kedudukan pesakitdan rawatan DIBH-RT.

INVESTIGATION OF TIME-OF-FLIGHT (TOF) IMAGING SYSTEM DURING DEEP INSPIRATION BREATH-HOLD RADIOTHERAPY (DIBH-RT) FOR LEFT BREAST CANCER PATIENTS

ABSTRACT

Deep inspiration breath-hold radiotherapy (DIBH-RT) pushes the heart away from treatment field thereby reducing the cardiac dose by over 50%. However, poor reproducibility and stability of the breath-hold during DIBH-RT treatment delivery could jeopardise the treatment success. The purpose of this work was to study the application of a Time-of-Flight (ToF) imaging system for monitoring breath-hold during DIBH-RT. Argos P330 3D ToF Camera (Bluetechnix Austria) was characterised by imaging an ISOCube phantom to assess the ToF measurement stability in conjunction with CBCT. Subsequently, the ToF imaging was performed on a total of 13 DIBH-RT patients during setup verification with CBCT imaging. Chest surface displacements were estimated from each modality and compared to validate the ToF measurement. The ToF imaging was also performed during the treatment delivery for evaluation of the breath-hold stability and reproducibility among the patients measured simultaneously with cine EPID imaging. The data were analysed using MATLAB (MathWorks, Natick, MA) and statistical tests were performed to evaluate the ToF accuracy. The intra-patient and inter-patient measurement stability of the ToF imaging system range from 0.05 to 0.31 mm and 0.68 to 0.74 mm, respectively, when assessed using the phantom. The absolute mean difference between ToF and CBCT was 0.28 ± 0.90 mm, and a correlation of 0.96 with a limit of agreement (LOA) of -1.49, 2.04 mm using phantom. The corresponding mean difference, correlation and LOA results obtained from patients were 2.88±5.89 mm, 0.92, and -7.36, 1.60 mm, respectively. The average correlation from all the fractions

obtained between ToF and EPID was -0.84. The average intra-field reproducibility were 2.70 mm, 1.37 mm, and 1.17 mm for lateral, medial and SCF fields, respectively. The average intra-fraction reproducibility and stability were 3.74 mm, and 0.80 mm, respectively, which is evidence of good reproducibility. The ToF imaging system shows good accuracy for monitoring breath-hold during DIBH-RT with a mean difference of 2.88±5.89 mm compared to CBCT which is within 10 mm margin used for breast treatment. Thus, it could be used safely during setup verification and treatment delivery for DIBH-RT.

CHAPTER 1

INTRODUCTION

1.1 Breast Cancer

In 2020, breast cancer remains the most common type of cancer in 159 of 185 countries including Malaysia, and only second to lung cancer in the remaining few countries (Sung *et al.*, 2021). A total of 2,261,419 new cases of breast cancer were diagnosed in 2020 which constitutes about 11.7 % of all cancer cases worldwide (Globocan, 2020). The total number of deaths due to breast cancer alone in 2020 was put as 684,996 (6.9%) worldwide (Sung *et al.*, 2021). The statistics in Malaysia show that breast cancer constitutes about 32.7% and 17.3% of all cancer cases among women alone and in both sexes combined, respectively (Bray *et al.*, 2018). The overall five-year survival rate for breast cancer patients in Malaysia is 49% (Abdullah *et al.*, 2013). It remains the second leading cause of cancer death in the country in 2020 (Globocan, 2020).

1.2 Radiotherapy Treatment for Breast Cancer

About 50% of cancer patients undergo radiotherapy during their treatment (Delaney *et al.*, 2005; Begg, Stewart and Vens, 2011). Radiotherapy involves the use of high energy x-ray in the MegaVoltage (MV) range to destroy the cancer cells. Breast cancer alone constitutes typically over 30% of the total workload in radiotherapy centres with the left breast being the most common (Beavis, 2006; Roychoudhuri, Putcha and Møller, 2006; Amer, 2014). Amer et. al., (2014) shows that the left breast cases constitute 50.9% while the right and bilateral cases were 46.1% and 3% respectively (Amer, 2014). A similar study reported 51.2% and 48% 0.8% for the left, right and bilateral respectively (Wennstig *et al.*, 2020).

Left breast cancer radiotherapy is associated with a significant risk of heart disease. Several studies including a meta-analysis revealed that the left breast patients compared to the right, have a higher incidence ratio of cardiac diseases after radiotherapy. The reported incidence ratio of the diseases with 95% confidence interval include pericarditis (1.61 [1.06-2.43]), acute myocardial infarction (1.22 [1.06-1.42]), angina (1.25 [1.05-1.49]), ischemic heart disease (1.09 [1.01-1.17]) and valvular heart disease (1.54 [1.11-2.13]) (McGale *et al.*, 2011; Cheng *et al.*, 2017; Wennstig *et al.*, 2020). This is because the heart lies immediate to the left chest wall which is part of the planning target volume (PTV) when treating the left breast cancer and thus, the heart inevitably is irradiated during the treatment (Bruzzaniti *et al.*, 2013; Kunheri *et al.*, 2017). The amount of dose received by the heart was found to correlate linearly with the risk of cardiac disease (Darby *et al.*, 2005). This prompted the development of techniques that would reduce the cardiac dose during left breast radiotherapy.

1.3 Cardiac Sparing Techniques During Left Breast Radiotherapy

There are two methods to ensure cardiac dose reduction during left breast cancer radiotherapy; irradiation of conformal beam to a small volume of the breast like accelerated partial breast irradiation (PBI) or the use of Intensity Modulated Radiotherapy (IMRT) and modification of the patient’s setup to displace the heart away from the radiation field/chest wall such as prone technique and breath-hold (BH); (Shah *et al.*, 2014). In PBI or IMRT, the treatment is restricted to the affected area by delivering a conformal beam only to the cancer target instead of irradiating the whole breast. IMRT delivers the conformal beam by varying the intensity of photons beamlets across the beam and deliver the treatment at multiple fixed gantry angles during each fraction. This was found to improve cardiac sparing compared to the whole breast irradiation technique (Hiatt *et al.*, 2006; Stewart *et al.*, 2008; Moon *et al.*, 2009). Nevertheless, this could not be used for all indications but least aggressive tumours.

Prone technique uses a special breast board to setup the patient in prone position during treatment which is not readily available. The technique only reduces the cardiac dose in about 50% of cases and can be worst in some cases (Kirby *et al.*, 2010; Huppert *et al.*, 2011; Lymberis *et al.*, 2012). Most recently, deep inspiration breath-hold radiotherapy (DIBH-RT) technique was reported as the most effective technique for cardiac dose reduction during left breast radiotherapy (Duma *et al.*, 2019). The technique requires the treatment to be delivered during deep inspiration breath-hold (DIBH) which pushes the heart away from the treatment field. DIBH-RT takes advantage of the separation between the heart and chest wall/field during DIBH which influences the cardiac dose. Several metrics describing the position of the heart relative to the field border or chest wall were established and were shown to correlate with cardiac dose. These include maximum heart distance (MHD) (Taylor *et al.*, 2009; Coon *et al.*, 2010; Qi *et al.*, 2012; Goody *et al.*, 2013; Conroy *et al.*, 2016; Wikström *et al.*, 2018), heart position to field edge (HP-FE) distance (Haaren *et al.*, 2017); and cardiac contact distance (CCD) (Hiatt *et al.*, 2006; Rochet *et al.*, 2015). The relative MHD from free breathing (FB) compared to DIBH in anterior-posterior (AP) and superior-inferior (SI) direction were 13.5 mm and 32.0 mm respectively (Yang *et al.*, 2015).

Several studies show that DIBH-RT reduces the cardiac dose compared to the standard FB radiotherapy (FB-RT) technique during left breast radiotherapy (Vikström *et al.*, 2011; Wang *et al.*, 2012; Bolukbasi *et al.*, 2014; Osman *et al.*, 2014). Comsa et al., 2014 reported up to 75% cardiac dose reduction with DIBH-RT compare to FB-

RT (Comsa *et al.*, 2014). The recommended mean cardiac dose in left breast tumour radiotherapy by the Royal College of Radiologists as contained in their guidelines is <2 Gy in 90% of total cases (Royal College of Cardiologists, 2016). Nonetheless, the success of the DIBH-RT technique relies on the reproducibility and stability of the BH during each treatment delivery. Figure 1.1 shows an illustration of chest surface position during FB, optimal and suboptimal breath-hold.

Breast radiotherapy is delivered in fractionated doses over several days or weeks (Yarnold, 2019; Braunstein *et al.*, 2020). Poor reproducibility and stability of the breath-hold during each fraction could lead to some geographic miss (Figure 1.2). This could result in poor dose distribution to the PTV and increased dose to the surrounding critical organs such as the heart, LAD; left anterior descending, and left lung which could compromise the treatment success. In view of these, several methods are introduced to aid accurate patient setup and or monitor the BH reproducibility and stability during DIBH-RT. These principally include imaging approaches such as the use of radiographic based imaging systems like CBCT and EPID for initial setup verifications, breath control method using Spirometry-based active breathing coordinator (ABC; Elekta AB, Stockholm, Sweden), and real-time tracking techniques with the use of video-based real-time position management (RPM; Varian Medical Systems, Palo Alto, CA) system, or commercial surface imaging system (SIS). Details of these systems can be found in Chapter 2.

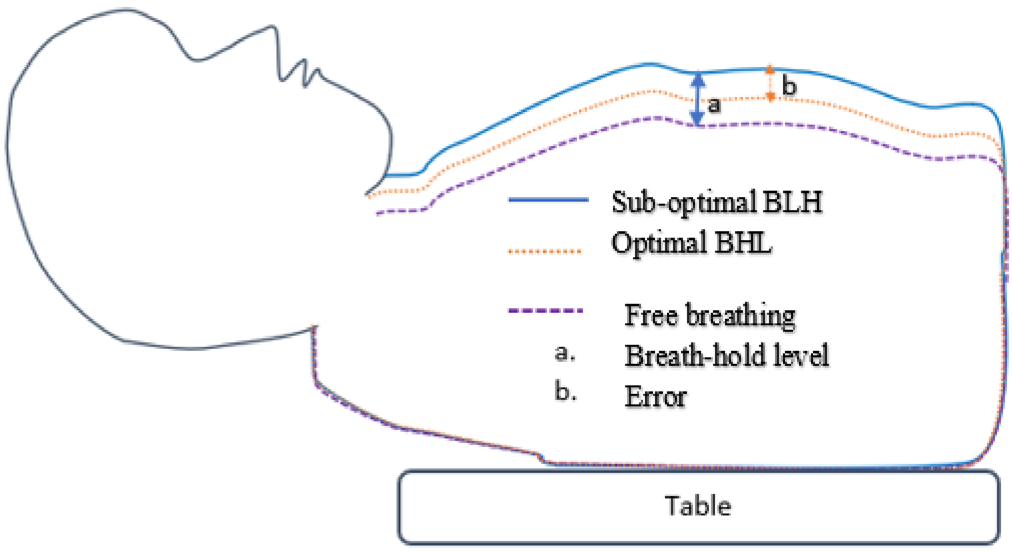

Figure 1.1 Chest surface position during FB, optimal and suboptimal breath-hold

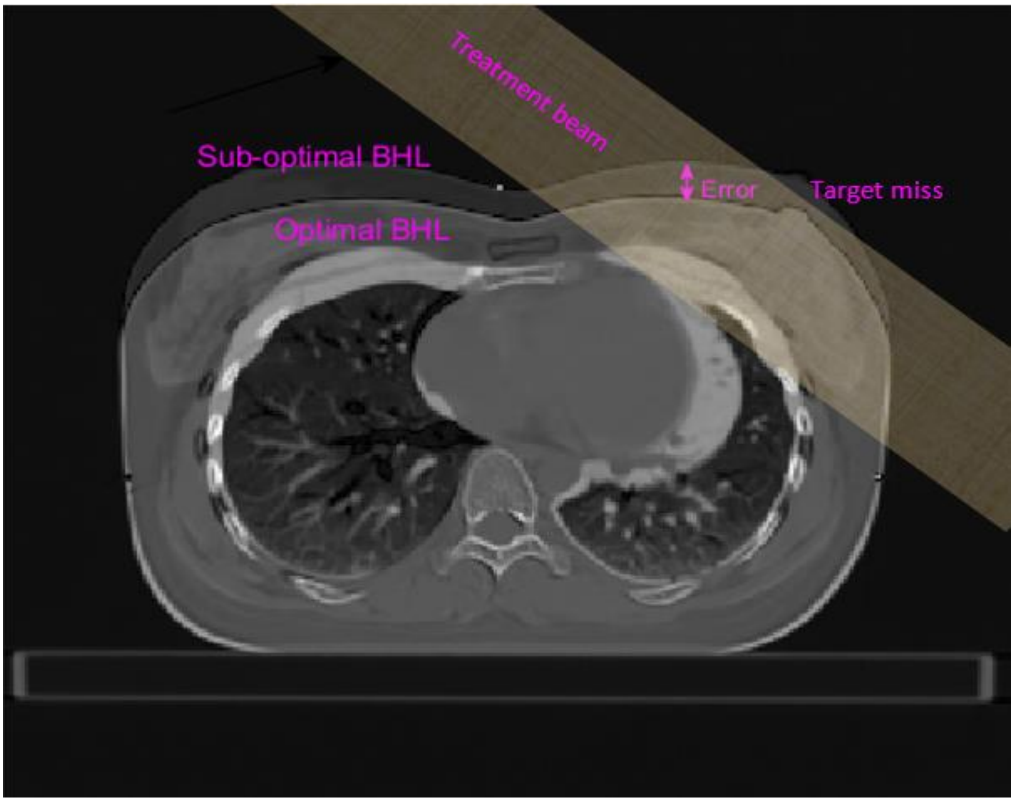

Figure 1.2 CT chest image during optimal and sub-optimal breath-hold level
Superimposed axial CT images of the chest acquired during optimal and suboptimal beath-hold. The chest surface, heart and breast occupy different positions on the two levels.

1.4 Setup Verification and Monitoring Techniques During DIBH-RT

The introduction of SIS for setup verification and breath-hold monitoring has revolutionised the DIBH-RT practice in recent years. The SIS is a non-radiographic imaging method that uses optical image sensors and light illuminator to provide images of the patient's surface at a designated frame rate. It is used as a contactless and ionising radiation-free method for real-time BH monitoring during DIBH-RT. Common commercial SISs are AlignRT (VisionRT, London, UK) and Catalyst (C-RAD, Uppsala, Sweden). The Catalyst uses camera-projector pair occupying a different viewpoint thus, suffers slight obstruction resulting in loss of depth data in some parts of the image (Foix, Alenyà and Torras, 2011). It has a frame rate of up to 200 fps.

AlignRT employs two cameras using a stereo setup and an additional light projector. It has a low frame rate ranging from 3-7 fps which may not be sufficient in detecting small abrupt motion. Overall, both systems are based on the triangulation working principle which strictly requires the stereo camera or camera-projector pair to be placed apart. This compromises the compactness of the system. Also, the baseline needs to be increased to allow accurate measurement at a longer working distance. Similarly, the triangulation-based systems have difficulty in measurements along sharp angles and small structures (Langmann, Hartmann and Loffeld, 2012). Further details about these systems can be found in Chapter 2. This work envisages that a SIS based on time-of-flight (ToF) technology has the potential to overcome the limitations of the existing commercial systems. The systems can also be costly and not commonly available in many radiotherapy centres.

1.5 Statement of the Problem

DIBH-RT offers a significant cardiac dose reduction during left breast radiotherapy. However, the success of this technique relies on good reproducibility and stability of the BH during each treatment delivery. The existing commercial SIS used for monitoring DIBH-RT are based on the triangulation working principle that has some limitations. The structured light based triangulation systems such as Catalysts used a camera-projector pairs which have different viewpoints resulting in loss of depth data (Foix, Alenya and Torras, 2011). Other triangulation systems such as AlignRT or Sentinel are based on stereoscopy and laser scanning techniques, respectively, which are associated with low imaging frame rates (Gilles et al, 2016; Hamming et al., 2019). These systems are less compact, thus, requiring a complex setup. Due to the relatively high cost, they are not available in many centres. The accuracy of the system also decreases at a longer working distance (Foix, Alenyà and Torras, 2011; Langmann, Hartmann and Loffeld, 2012; Kim and Lee, 2013). Owing to these limitations, attention has been shifted to imaging systems based on ToF technology.

The ToF imaging system provides image of an object based on the distance from the sensor to the corresponding point on the object. Each pixel in the image maps the distance information based on the light travel time from the illuminator to the object and back to the sensor co-positioned with the illuminator. Unlike the commercial SIS based on triangulation, the illuminator and the sensor have the same viewpoint eliminating the problem of partial obstruction and depth data loss. This arrangement could as well facilitate the construction of a compact system that does not require a complex setup in the treatment room and provide an accurate measurement at a longer distance irrespective of the baseline.

Several studies have explored the application of ToF imaging systems in radiotherapy for patient setup or real-time motion monitoring. However, majority of the studies involved only phantom data which does not reflect the patient characteristics in clinical situation such as voluntary motion or motion due to heartbeats, coughing and sneezing (Edmund et al. 2016; Nazir et. al., 2018; Ulrich et al., 2010; Placht et al., 2010; 2012; Schaller et al. 2009). Studies from Schaller, Penne and Hornegger, (2008) and Silverstein and Snyder, (2018) involved human volunteers but did not involve breath-hold. Also, a respiratory belt was used to provide the ground truth which lacks the dimensional information.

To the best of my knowledge, Edmund et al. 2018 was the only study that utilised a ToF camera (Microsoft Kinect v2) during breath-hold to evaluate the feasibility of gating the linac treatment delivery, but its accuracy was not evaluated in the study. The study acquired signal from human volunteers during breath-hold which was used on a motion platform to simulate DIBH-RT. All data were collected on the same day which may not reflect day-to-day variation in the environment due to temperature fluctuations that could occur during clinical practice. The study focused on VMAT technique which involves gantry rotation during treatment delivery. The authors noted that the depth measurement changes by up to 7 mm as the gantry rotates. This could be due to gantry rotation associated with VMAT technique since the measurement was performed on a static target. This error was not investigated further nor attempted to be corrected. The gantry error, if not corrected would not allow for breath-hold monitoring during 3D-CRT as the breath-hold reading would vary at different gantry angle. Finally, no study evaluated the breath-hold reproducibility and stability during DIBH-RT using the ToF camera.

1.6 The Hypothesis of the Study

This work hypothesises that a SIS based on ToF technology has sufficient accuracy to detect surface displacement and could be used for BH monitoring during DIBH-RT for left breast cancer. This will utilise the advantage of the off-the-shelve technology as a contactless, non-invasive BH monitoring method with real-time imaging capability without concomitant imaging dose.

1.7 Objectives of the Study

This work aims to investigate the application of a ToF imaging technology for monitoring DIBH-RT for left breast cancer patients. The specific objectives are as follows.

1. To measure the accuracy and the uncertainties of the ToF imaging during DIBH-RT application using phantom.
2. To estimate the setup uncertainties among left breast cancer patients during DIBH-RT based on CBCT images obtained during the treatment.
3. To evaluate the performance of the ToF imaging for set-up and intrafraction monitoring using CBCT and EPID as goal standard, respectively.

1.8 Thesis Structure

Chapter 1 introduces the recent breast cancer statistics such as the incidence, mortality, and survival rate. The common cardiac sparing techniques during left breast radiotherapy including DIBH-RT are also explained. The problem statement and motivation to study the application of the ToF imaging system in monitoring BH during DIBH-RT are discussed. The objectives of the thesis, as well as the hypothesis, are also presented in the chapter. Finally, the thesis structure was presented.

Chapter 2 gives a detailed working principle of ToF imaging. Several studies that characterised the ToF imaging system for various applications including patient's setup and motion tracking in radiotherapy are discussed. The studies showed that the performance of the ToF imaging system depends on the application of interest. Thus, the need to characterise the system for any intended application forms the basis of the characterisation study in Chapter 3. The systems based on similar technology such as stereoscopy and structured light as well as their working principle and limitations are also discussed. These include commercial SIS such as AlignRT and Catalyst. Several studies that evaluated the accuracy of these systems using radiographic imaging as a reference standard are discussed. The recommendation of these studies that SIS should be used in conjunction with radiographic-based system informed the decision to characterise the ToF using CBCT as a reference. Radiographic-based systems conventionally used for initial setup verification during DIBH-RT and other DIBH-RT monitoring techniques such as ABC and RPM are also described in this chapter.

Chapter 3 focuses on the characterisation of the ToF camera for the DIBH-RT application. The performance of the ToF camera in terms of intra-patient and inter-patient measurement stability are investigated. The chapter also investigates the accuracy of the ToF imaging system in the detection of surface displacement using phantom. In addition, the chapter investigates scene-dependent factors that could impact the measurement accuracy of the ToF imaging during DIBH-RT. These include gantry rotation during CBCT imaging for setup verification, variation in static gantry head position during treatment delivery in a single fraction for 3D-CRT as well as radiation exposure. Finally, the chapter evaluates the accuracy of the CBCT system in the detection of surface displacement. This is to estimate the system uncertainty before clinical application in conjunction with the ToF imaging system. However, this does not include the uncertainty coming from the patient which is discussed in Chapter 4.

Chapter 4 focuses on the estimation of the setup uncertainty among left breast DIBH-RT patients using CBCT. This is to estimate the setup uncertainty and PTV margin using the traditional IGRT method before the application of the ToF imaging system. This is to ensure that the adopted PTV margin is optimal for DIBH-RT in the centre as it will be used as the basis for interpretation of the ToF accuracy. The accuracy of the ToF must be well within the PTV margin before it could be accepted. At the onset, the CBCT and treatment isocentre congruence is evaluated. The patient setup uncertainty and PTV margin for offline (NAL; No action level and eNAL; Extended no action level) and online IGRT protocols are estimated. A new calculation method using MATLAB algorithm was used to calculate the error and PTV margin.

Chapter 5 evaluates the accuracy of the ToF imaging system for measurement of DIBH-RT setup verification using CBCT as a reference. An algorithm to render the surface of CBCT images and extracts of the patient surface depth (PSD) within the selected ROI is developed in this chapter. This extracts the PSD information on the CBCT image of the same size and location of the corresponding ROI selected on the ToF images. A similar algorithm was developed that extracts the ROI depth image from the ToF images. However, there is a need to further evaluate the accuracy of the ToF imaging during treatment delivery as the scene varies for each treatment field due to variations in gantry angle.

In Chapter 6, the ToF accuracy during DIBH-RT delivery is evaluated using EPID imaging as a reference. This is achieved by comparing the measurements from the ToF with EPID in continuous imaging mode (cine EPID). Two methods for correction of the impact of gantry angle on the ToF imaging are developed in this chapter. This is to correct for the impact of gantry head position/angle on the ToF imaging observed in the characterisation study in Chapter 3. This could allow for the estimation of breath-hold reproducibility during each fraction. The impact of location and size of the regions of interest (ROI) used on the breath-hold reproducibility are evaluated. Finally, the intra-field reproducibility, intra-fraction reproducibility, and BH stability among left breast patients treated using DIBH-RT are evaluated. Chapter 7 constitutes a summary of the work, conclusion, and recommendations on areas for further research.

CHAPTER 2

LITERATURE REVIEW

2.1 Introduction

Radiotherapy is the treatment of abnormal cells or cancer using x-rays. A high dose of x-rays creates chemical changes that damage the deoxyribonucleic acid (DNA) within the cells of biological tissues through which it traverses. This affects the function of the cells leading to halting further growth or death. Radiotherapy uses specialised equipment, typically a linear accelerator (linac) to deliver a high radiation dose to the tumour cells while sparing the surrounding normal tissues. The radiotherapy process starts with patient consultation at the clinic by a specialist doctor followed by CT simulation, treatment planning, setup verification, and treatment delivery as discussed in detail in Chapter 4. This work focuses on the setup verification aspect which involves the use of imaging to check the patient's position just before and or during the treatment delivery. Although several imaging techniques are being used for setup verification, a lot of interest has been developed in the use of SIS in recent years.

The use of optical SIS has created a paradigm shift in DIBH-RT practice. This chapter gives a detailed theoretical background of the ToF imaging system which is the main focus of this work. These include the basic principle, main components, and applications of the ToF system as well as its technical performance. Several studies that characterised other commercial ToF systems are discussed, and the common sources of measurement error are highlighted. A number of studies on the use and potential of the ToF system for radiotherapy applications using phantoms and patient data are also presented. The basic principle of other optical systems based on similar technology such as stereoscopy and structured light and their performance in SGRT are also included in this chapter. Radiographic-based systems such as EPID and CBCT as well as other non-radiographic systems like ABC and RPM used in monitoring DIBH are also included.

2.2 Time-of-flight (ToF) Optical Imaging Technology

ToF imaging technology provides depth or distance images of the objects and the entire scene within a specified field-of-view (FOV). It works by calculating the light travel time from the illuminator unit to the object/scene and back to the sensor co-positioned with the illuminator (Brahme, Nyman and Skatt, 2008; Bamji *et al.*, 2015). The imaging systems based on this technology are commonly called the ToF camera. This camera provides both depth and amplitude images at a high frame rate making it suitable for real-time imaging applications. The depth image provides the "depth" or z-axis information of the imaged object. This represents the distance of the object from the camera. The amplitude image gives the amount of signal reflected from the imaged object. Each pixel reflects the amount of signal intensity received from the corresponding point in the scene.

2.2.1 Major Components of the ToF Imaging System

The ToF imaging system mainly consists of an illumination unit, lens and a sensor. A simple diagram illustrating the arrangement of the major components of the ToF camera is shown in Figure 2.1. The commonly used illumination units are light amplification by stimulated emission of radiation (laser) or light-emitting diode (LED) device which serves as a source of near-infrared (NIR) light for scene illumination. The NIR is chosen due to the advantage of less interference with the visible light presence in the environment most especially during outdoor application (Bamji *et al.*, 2015). Laser or LED is required because the light needs to be modulated at a high speed up to 100 MHz which is difficult to be achieved with other devices. The typical NIR light used for ToF application operates at 850 nm or 940 nm wavelength which are both available with laser and LED illuminators. The quantum efficiency of the sensor is better at 850 nm wavelength, thus leading to lower noise and high precision. However, NIR at 850 nm can be visible most especially in the dark while at 940 nm is completely invisible and thus, remains the best choice for applications involving the face.

The lens is one of the essential components of the ToF camera that focuses the reflected light from the scene to the sensor and ensures that every light coming from a point in the scene incident on a given pixel. As the ToF camera works based on active illumination, the lens aperture and transmission efficiency are designed to allow the light within the wavelength of interest to reach the sensor (Sadhu, 2016). This helps to reduce the impact of ambient light on the depth measurements.

The sensor consists of closely packed pixels arranged in a 2D array of hundreds or thousands of pixels per column or row. It is a solid-state semiconductor device that converts the incident light signal into digital numbers. At first, the incident light photons are converted into photoelectrons. The accumulated charges in each pixel are then converted to voltages and the resultant analogue signal is subsequently converted to digital numbers by an analogue-to-digital converter (ADC). The common sensors used in ToF technology are charge-coupled devices (CCD) and Complementary Metal Oxide Semiconductor (CMOS) image sensors. Both devices have photodiode in each pixel to convert the light into electrons, however, the manufacturing process and the readout method varies.

In a CCD image sensor, the reflected light is detected at each pixel and converted to photoelectron. The electrons then move from pixel to pixel to one end of the sensor for readout by a single readout amplifier. Thus, the readout is extremely consistent due to the use of a single readout amplifier, but the process is slow as the electrons must move to one end of the device. For the CMOS image sensor, each pixel is equipped with transistors and a readout amplifier, thus the readout process is performed in each pixel and simultaneously, making the process faster (Kitagawa, Scheetz and Farman, 2003). The fast readout capability of the CMOS image sensor and the lower cost makes it dominant over the CCD sensor.

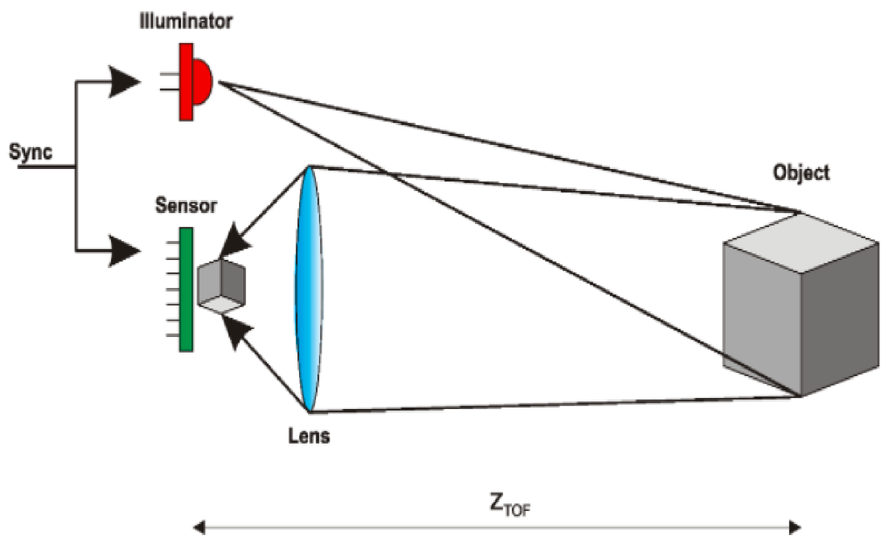

Figure 2.1 Schematic diagram of the arrangement of major components of the ToF camera (DeCode, 2020).

2.2.2 Working Principle of the ToF Imaging System.

Depth measurement using ToF technology involves the measurement of light travel time from the illuminator to the object and back to the sensor. This could be achieved via two methods; pulse-based ToF (PB-ToF) and amplitude modulated continuous wave ToF (AMCW-ToF) measurement methods (Niclass *et al.*, 2005; Stoppa *et al.*, 2007; Bamji *et al.*, 2015; Sarbolandi, Plack and Kolb, 2018).

2.2.2(a) Pulse-based ToF (PB-ToF) Method.

PB-ToF measurement method involves the direct measurement by a precise timer, of the duration for the short light pulse emitted by the illuminator to be reflected and detected at the sensor (Stoppa *et al.*, 2007). When a reflected signal is first detected, a trigger signal is generated to halt the time measurement (Stoppa *et al.*, 2007). Since the speed of light, c is constant (3.0×10^{8} m/s), the distance, d can be calculated using Equation. 2.1. This method is also known as the stopwatch technique (Bamji *et al.*, 2015).

$$d = \frac{c\Delta t}{2} \tag{2.1}$$

The PB-ToF method allows distance measurement of up to several kilometres (Niclass *et al.*, 2005; Stoppa *et al.*, 2007). In addition, it has less intensity-relate error than the AMCW-ToF while the multipath interference of the two methods is comparable (Sarbolandi, Plack and Kolb, 2018). However, this method requires an extremely high accurate timer to estimate the runtime of the light pulse. These are very expensive and could make the total cost of the sensor very high (Lachat *et al.*, 2015). In addition, the on-chip time-to-digital converter (Markovic *et al.*, 2013) or time-to-amplitude converter (Crotti, Rech and Ghioni, 2012) used with this method occupies a large pixel area and thus, requires the use of larger pixel size, limiting the pixel array size (Bamji *et al.*, 2015). As small as 4 × 64 and 32 × 32 pixel array size with 130 × 300 μm^2 and 58 × 58 μm^2 pixel size respectively, were reported using this method (Schrey *et al.*, 2003; Niclass *et al.*, 2005). The reduced number of pixels could result in low lateral resolution.

2.2.2(b) Amplitude Modulated Continuous Wave ToF Method.

AMCW-based ToF measurement method involves the calculation of distance based on the phase shift between the emitted and reflected light. The AMCW-ToF was discussed extensively in the literature (Foix, Alenyà and Torras, 2011; Li, 2014; He *et al.*, 2017; Sarbolandi, Plack and Kolb, 2018; He and Chen, 2019). This is summarised as follows. The AMCW-ToF method modulated continuous wave is used to illuminate the scene during which four samples are taken for every period each phase-stepped by 90°. For instance, the sample can be taken at four sampling windows, C1, C2, C3, and C4 corresponding to the 90°, 180°, 270°, and 360° respectively (Figure 2.2). This is known as the four-bucket technique. The charge accumulated during each sampling, Q1, Q2, Q3, and Q4 for the respective sampling windows are used to compute, in each pixel, the phase shift, φ, between the incident and reflected light (Equation 2.2). The offset, B as well as the amplitude, A can be obtained using Equations 2.3 and 2.4, respectively. The calculated phase shift is subsequently used to calculate the target-to-sensor distance, d using Equation 2.5.

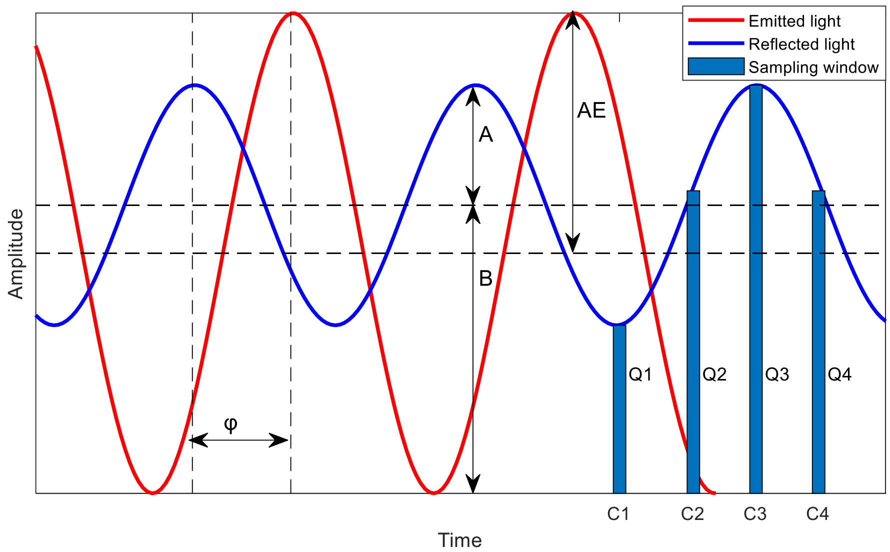

Figure 2.2 AMCW-ToF measurement method

$$\varphi = \arctan\left(\frac{Q3-Q4}{Q1+Q2}\right) \quad 2.2$$

$$B = \frac{Q1+Q2+Q3+Q4}{4} \quad 2.3$$

$$A = \frac{\sqrt{(Q1-Q2)+(Q3-Q4)}}{2} \quad 2.4$$

$$d = \frac{c}{4\pi f}\varphi \quad 2.5$$

2.2.3 The Technical Performance of ToF Imaging System

Several ToF cameras from different manufacturers are available in the market. The common manufactures of commercially available ToF cameras include Swiss ranger, E-series, Cam Cube and Microsoft. Figure 2.3 shows typical ToF cameras from different manufactures. Although all the cameras are based on ToF technology, some of their features vary. These include the resolution/array size, FOV size, maximum range measurement, and maximum frame rate. Thus, ToF cameras from different manufactures or the same manufacture but of different versions could exhibit different technical performance due to the variation in the above-mentioned parameters. The features of the common commercial ToF camera are given in Table 2.1.

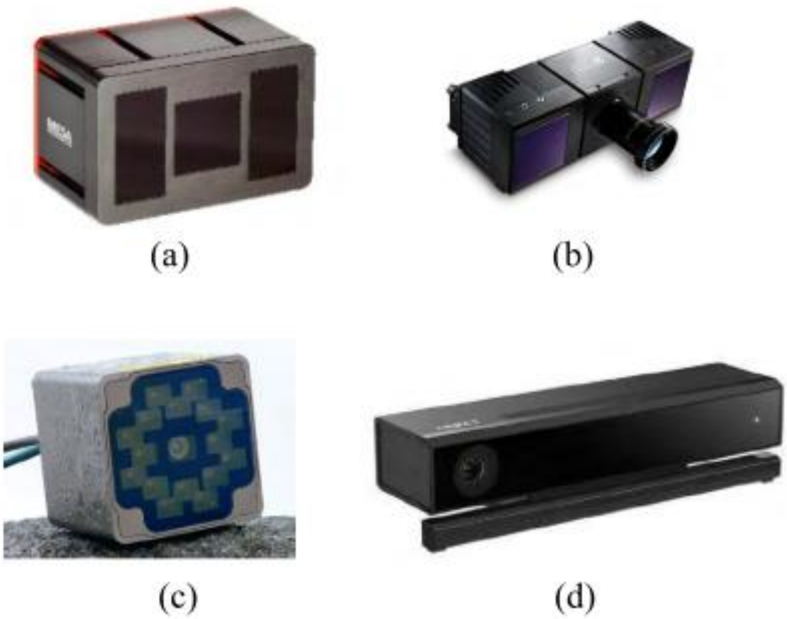

Figure 2.3 Typical commercial ToF cameras. SR 4500 (a), CamCube 3.0 (b), E-series 70 (c), and (d) Microsoft Kinect v2.

Table 2.1 Features of common commercial ToF imaging systems

ToF Camera	Year	Resolution	Maximum frame rate (fps)	FOV (Degrees)	Measurement range (m)
Mesa 4500	2008	176 × 144	30	44 × 35	Up to 9.0
PMD	2010	200 × 200	40	40 × 40	0.3 to 7
Fotonic E70	2012	160 × 120	58	70 × 53	0.15 to 10
Microsoft	2013	512 x 424	30	70 × 60	0.5 to 4.5

Several factors are known to affect the performance of the ToF cameras which include but are not limited to temperature, distance, and scene-related factors. The temperature-related error is due to the changes in the properties of the semiconductor-based sensor device in response to the changes in temperature. This causes distance drift in the pixels until the temperature is stable. To avoid this error, ToF sensors can run for some time after the switch on, to ensure the temperature is stabilised before they are put into daily use. This waiting period is known as warmup time and it varies among different ToF camera models (Fursattel *et al.*, 2015; Lim and Zin, 2018). The distance-related error which is also known as wiggling error results due to imperfection in the generation of the NIR modulated light that is used for scene illumination. This imperfection results in an offset that solely depends on the measured distance (Foix, Alenyà and Torras, 2011). Change in the integration time was also reported to affect the absolute distance measurement instantly and followed by gradual drift for a few minutes before it gets stabilised (Foix, Alenyà and Torras, 2011; Fursattel *et al.*, 2015).

Several studies have explored these sources of errors on different ToF cameras, and the error results were used as a basis to characterise the performance of different ToF cameras (Guomundsson, Aanæs and Larsen, 2007; Weyer *et al.*, 2008; Fursattel *et al.*, 2015; He *et al.*, 2017; Lim and Zin, 2018). The studies concluded that it is difficult to identify one of the ToF cameras as best for all applications. Some cameras perform better for a specific application but perform poorly for other applications. Thus, the selection of the camera should be based on the intended application and should be characterised for that purpose before use or each time the condition is changed. This is the basis for chapter three of this thesis which involves the characterisation of the ToF camera for the DIBH-RT application.

2.2.4 Application of ToF Imaging System in Radiotherapy

A number of studies have explored the application of the ToF camera in radiotherapy patients' setup and respiratory motion gating/tracking. Schaller et. al., 2008 pioneered the investigation of the ToF camera for radiotherapy application with a specific interest in respiratory motion gating (Schaller, Penne and Hornegger, 2008). The ToF imaging was performed synchronously with measurements from an ANZAI respiratory belt (AZ-773V, ANZAI Medical Co.). The measurement was performed on 13 human subjects and a mean correlation coefficient of 0.88 between the ToF and the respiratory belt was achieved (Schaller, Penne and Hornegger, 2008). However, this study only provided correlation results which does not reflect the actual accuracy of the ToF camera. Also, the ToF camera in this study provided motion information in the AP dimension while the respiratory belt does not specify any dimension. A similar study also shows that the measurement from a Kinect v2 ToF sensor correlated well with measurements from ANZAI belt and RMP (Silverstein and Snyder, 2018).

A study by Ulrich *et al.*, (2010) evaluated the dynamic accuracy of the ToF camera using different breathing frequencies ranging from 3 to 25 min^{-1} and amplitudes of 1.3 to 18 mm. The authors employed the use of a plaster cast human torso phantom with an in-built mechanism that allows simulation of human respiratory motion. This was used to provide the ground truth measurements. The results showed that a correlation coefficient of 0.65 and 0.80 were achieved with respiratory motion amplitude of 1.5 mm and amplitude greater than 5 mm, respectively. Furthermore, Placht et al. 2012 presented a fast ToF surface image registration algorithm with a temporal lag of only 65 ms in the registration outcomes making it suitable for dynamic or gating studies (Placht *et al.*, 2012).

A similar study by Edmund et al., the motion of a dynamic phantom was monitored using Kinect v2 ToF camera and a Leica Disto D210 laser device (Leica Geosystems AG, St. Gallen, Switzerland) mounted securely and in line with the ToF camera to provide the ground truth. The phantom motion was in two sinusoid trajectories each with a peak-to-peak amplitude of 20 mm over a duration of 12 s and then 2 sec. The results show the root mean square error of 1.4 and 1.1 mm for the trajectories of 12 sec and 2 sec respectively. The study also shows that the tracking capability is not affected by electromagnetic interference and radiation exposure during the linac operation. Nevertheless, this study did not investigate the impact of variation in reflected IR signal due to change in background scene with change in gantry head position or rotation. Also, all the studies used phantom and did not involve human subjects to reflect the actual error that would occur if patients were involved. Involuntary motion such as cough or sneezing might occur with human subjects which are not considered in these studies.

On the other hand, several other studies explored the feasibility of using the ToF camera for radiotherapy patients' setup (Schaller *et al.*, 2009; Placht *et al.*, 2010, 2012). Schaller et al. (2009) used a robotics arm with a precision of 0.1 mm and 0.1° in translational and rotational dimensions and a rigid torso phantom to simulate the setup errors. The mean positioning accuracy of the ToF camera achieved was 2.88 mm and 0.28° in the translational and rotational direction, respectively. The study was extended to three human subjects and the accuracy obtained was 3.38 ± 2.0 mm

(Schaller *et al.*, 2009). In this study, the camera was mounted rigidly above the treatment couch, such that it is perpendicular to the target. This is not feasible in true clinical settings as the gantry could obscure or collide with the camera when the treatment head is at a 360° gantry angle. This could be an issue if this setup were to be translated into the radiotherapy clinic.

The same research group in the study of Schaller et. al. 2009 introduced three pre-processing steps and distance calibration to improve the results obtained in their previous study (Placht *et al.*, 2010). These steps include bilateral filtering, temporal averaging, and variance filtering to reduce spatial noise, temporal noise, and ‘’flying pixels’’ respectively as they could impact the registration accuracy. The authors used a plaster cast-based rigid torso phantom to simulate the patient’s setup error. Three gauges were used to monitor the position of the table each in one translational direction to provide the ground truth. The mean registration error obtained was 0.74±0.37 mm. However, the shifts applied were only within 9.5 mm due to the limitation of the gauge. The mean errors obtained for 0.5 and 9.5 mm shifts were 0.3 and 1.75 mm, respectively. This shows that the magnitude of the errors increases with the magnitude of the displacement. Thus, a mean error larger than 0.74±0.37 mm reported in the study might occur if displacements of >10 mm were applied which is likely during a true clinical scenario. Also, the authors monitor the table movement as a surrogate of the phantom displacement which is likely to introduce error. Likewise, the camera setup was perpendicular to the target as in their previous study (Schaller *et al.*, 2009).

Furthermore, the research group developed a more advanced rigid registration algorithm that allowed registration accuracy sufficient for radiotherapy setup even with large displacements (Placht *et al.*, 2012). The registration algorithm developed involves distance calibration and Kalman filtering as pre-registration steps to enhance spatial accuracy and reduce temporal noise, respectively. Also, the issue of camera setup in the previous studies was solved by mounting the camera on the ceiling focussing on the treatment table at an incident angle of 78°. The ground truth was provided by the couch control system instead of the gauge that is limited to 10 mm. The mean accuracy achieved was 1.62 ± 1.08 mm and 0.07° ± 0.05° for translational and rotational direction, respectively. This is less than what was achieved by Schaller et al. 2009 (3.38 ± 2.0 mm) (Schaller, Penne and Hornegger, 2008). However, it is larger than what the authors reported in their previous study (0.74 ± 0.37 mm) (Placht *et al.*, 2010). This is perhaps because the most recent study employed translational deviation of much larger than 10 mm and a working distance of 1200 mm compared to 800 mm used in the previous study. Also, additional uncertainty could result due to camera angulation. The motion in the phantom is in true AP dimension while the camera measures at an angle of 78°. The authors did not mention how this was compensated. Another limitation of this study is the use of the only phantom without supplementary data from human subjects to mimic true clinical scenarios.

In a quest to further improve the accuracy of the ToF, two studies compared the use of two stereo-ToF systems in patients' setup and a single ToF camera (Wentz *et al.*, 2014; Gilles *et al.*, 2016). In the study of Wentz et al. 2014, a linear actuator was used to produce a precise and reproducible position of the phantom to provide the ground truth. The reference and displaced positions were captured using a single ToF camera and the ToF stereo systems. The measurements were repeated on a volunteer and subsequently on patients undergoing radiotherapy treatment. The use of two ToF cameras shows better results compared to a single camera for phantom displacement greater than 10 mm. Similar results were obtained from the patients' data regardless of the magnitude of the displacement applied. The results show that errors of 1.5 mm